

Processing Three-Channel SAR-ATI for GMTI

J.E. Barker ^{#1}, B.C. Barber ^{#2}

[#] *Sensors and Countermeasures Department, Dstl
Building 5, Dstl Porton Down, Salisbury, Wiltshire, SP4 0JQ, UK*

¹ JEBARKER@dstl.gov.uk

² BCBARBER@dstl.gov.uk

Abstract—This paper investigates two methods for GMTI using three-channel SAR-ATI data. Motivated by previous results in the two-channel case, a deterministic method for finding an Eigendecomposition of the SAR-ATI sample covariance matrix is presented. The CFAR detection capability of each of the eight parameters of the Eigendecomposition is evaluated using measured three-channel airborne data and compared to the well-known DPCA-ATI metric. Results suggest that all moving target energy is contained in a single parameter, the largest Eigenvalue, and that for a given theoretical CFAR a lower real-world false alarm rate is achieved in comparison to DPCA-ATI. Motivated by this result ICA is then applied to the same measured three-channel data and found to both detect and distinguish two different types of moving target simultaneously present in a maritime environment.

I. INTRODUCTION

A. Problem Statement and Motivation

The ‘classical’ way to detect and track ground moving targets using an airborne radar is by using a Ground Moving Target Indicator (GMTI) radar. Conventional moving target indication (MTI) radars already provide the required wide area surveillance for battlefield situational awareness applications; however, they cannot have a sufficiently fine resolution, geo-location accuracy or minimum detectable velocity to provide all required functions arising as a result of the changing operational environment. For example, there is a need to engage small, slow-moving targets in cluttered radar environments and identify the targets. The high spatial resolution imaging provided by a synthetic aperture radar (SAR) system is required to maximise the probability of detection of such targets, albeit with a reduced area of sensor coverage. Future SAR systems have active array antennas which can give multiple beams along the aircraft track that can be set up as a SAR interferometer. In theory, combined processing of the signals received by each antenna in the array could result in fine resolution SAR images in which the stationary background is greatly attenuated leaving only the moving targets. However, there is currently no general theory to guide the best way of processing the signals from such systems for more than two beams when there are many different types and classes of scatterer.

B. Mathematical Problem Formulation and DPCA-ATI

Consider a side-looking airborne radar sending out coherent, large bandwidth pulses while it moves along its track. At

some point on the time scale of the pulse repetition frequency (PRF) a pulse will reflect off a target and return to the radar. The reflected pulse is measured as an amplitude and a phase. In the absence of sensor noise, the phase of the returned pulse depends only on the radar wavelength and the distance between the target and the radar. The relative speed of the airborne platform to the speed of light is small enough to consider the platform stationary over the time taken for a pulse to be sent out and returned. The measured reflected signal can be represented by the complex quantity $z_1(t)$ where t is the time at which the measurement is made. $z_1(t)$ can be modelled as a complex zero-mean stationary Gaussian process. Justification for this model can be found in [1].

After a short period of time, δt , the measurement is repeated with the radar at the same location as before. This can be achieved by having a second trailing antenna attached to the airborne platform in the along-track direction. The signal measured by the second antenna will be $z_1(t + \delta t)$ where the range from the antenna to target $r(t + \delta t)$ may be different from $r(t)$ due to target motion.

If N antennas are arranged along-track in the same fashion the corresponding returned signals, $z_1(t), \dots, z_N(t + N\delta t)$, may be obtained as each antenna moves into the same position over time.

The sample covariance matrix of n identically distributed k -element random vectors is defined as

$$\hat{\mathbb{R}}_{zz} = \frac{1}{n} \sum_{m=1}^n \underline{z}(m) \underline{z}(m)^H \quad (1)$$

where H denotes Hermitian transpose and $\underline{z}(m)$ represents a sample of the k -element random vector, i.e. $\underline{z}(m)^H = [z_1(m)^* z_2(m)^* \dots z_k(m)^*]$, and $*$ denotes complex conjugation. The sample covariance matrix is a natural way of processing n -look k -channel SAR signals (in the SAR multi-look processing sense) and gives the maximum likelihood estimator for the elements of the covariance matrix of the received signals. The covariance matrix is the fundamental object of interest as, in theory, the phase changes between the signals received through different channels contains the information required to differentiate moving targets from the static (or modelled moving) background.

Let $\hat{\mathbb{R}}_{zz}(i, j)$ denote the element of $\hat{\mathbb{R}}_{zz}$ on row i and column j . The argument and magnitude of $\hat{\mathbb{R}}_{zz}(i, j)$ are called

the ATI phase and amplitude of the channels i and j . In the absence of thermal and sensor noise, a non-zero ATI phase indicates that the observed target has moved between being observed by channels i and j . The variance of the phase sample defines a limit on the lowest speed at which the target is detectable since the ATI phase is proportional to target across-track speed.

The quantity

$$DPCA_{ij} = \hat{\mathbb{R}}_{zz}(i, i) + \hat{\mathbb{R}}_{zz}(j, j) - \hat{\mathbb{R}}_{zz}(i, j) - \hat{\mathbb{R}}_{zz}(j, i) \quad (2)$$

defines the displaced phase centre array (DPCA) metric between channels i and j and is a commonly used moving target metric. One expects that the radar returns of two channels observing a target that does not change will be identical and so, similarly to the ATI phase, the DPCA metric should return zero. However, if the target does change between measurements then the subtraction will give a non zero result.

Both of the above metrics are defined in a pairwise fashion between SAR channels. For a three-channel system a compound metric can be defined in the following way:

$$ATI_{123} = \arg(DPCA_{12}DPCA_{23}^*). \quad (3)$$

Clearly this metric is the ATI phase between the DPCA metrics of channels 1 and 2 and channels 2 and 3. An automatic constant false alarm rate (CFAR) detector can be realised by computing an appropriate threshold for ATI_{123} given the tolerable rate of false alarms and knowledge of the statistics of this metric. For a theoretical analysis of the performance of this metric see [2].

II. EIGENDECOMPOSITION PARAMETERS AS GMTI METRICS

In the case of a two-channel SAR-ATI system, Sikaneta and Chouinard [3] showed that the joint probability density function (p.d.f.) of the four parameters of the Hermitian sample covariance matrix, a Wishart distribution, can be transformed into a joint p.d.f. of the two Eigenvalues, a rotation angle and the ATI phase. This was accomplished by means of a unitary transformation in the group $U(2)$. This decomposition allowed the marginalisation of the four parameter joint p.d.f. by each parameter. These marginalisations allowed the computation of constant false alarm rate (CFAR) GMTI detection thresholds for each parameter. As a result a new detection metric, the adaptable hyperbolic detector, was constructed as a product of two of the transformed parameters and was demonstrated on real and synthetic data to be a more effective GMTI metric than both DPCA and the ATI phase.

Motivated by this approach we present an equivalent decomposition of the three-channel covariance matrix $\hat{\mathbb{R}}_{zz}$. Since $\hat{\mathbb{R}}_{zz}$ is Hermitian there exists a unitary matrix U such that $U^{-1}\hat{\mathbb{R}}_{zz}U = \mathbb{E}$ where \mathbb{E} is the diagonal matrix of Eigenvalues of $\hat{\mathbb{R}}_{zz}$. It can be shown that the parameters $\theta, \phi, \psi, \delta_1, \delta_2$ can be deterministically calculated from the elements of $\hat{\mathbb{R}}_{zz}$ so that U takes the form shown in Equation 5.

Anastassakis [4] presented a geometrical method for diagonalising a real symmetric 3×3 matrix. Anastassakis's solution uses Euler rotations to attain analytical expressions for the Euler angles (parameters of the diagonalising rotation matrices) and Eigenvalues in terms of elements of the symmetric matrix. The problem of calculating the matrix U to diagonalise the three-channel SAR sample covariance matrix is the Hermitian analogue to the symmetric matrix diagonalisation solved by Anastassakis. By first applying the transformation matrices P^1 and P^2 shown in Equation 5 with phase parameters given by

$$\begin{aligned} \delta_1 &= (\phi_2 - \phi_1)/3 \\ \delta_2 &= -(2\phi_2 + \phi_1)/3 \end{aligned} \quad (4)$$

the arguments of the exponential terms of the Hermitian covariance matrix are annihilated leaving a real symmetric matrix. Anastassakis's method can then be directly applied to calculate the three rotation angles θ, ϕ and ψ and the Eigenvalues λ_1, λ_2 and λ_3 .

It is an open research question to derive analytical expressions for the marginal p.d.f. of each of the Eigendecomposition parameters. In the absence of these marginal distributions we must estimate CFAR detection thresholds by using simulated SAR clutter data to approximate each p.d.f. This simulation is presented in Section III-B.

III. EXPERIMENTAL SAR DATA

A. ESR Data

In this work three-beam SAR data obtained by the experimental airborne Enhance Surveillance Radar (ESR) is used to both estimate the covariance matrix parameters required for synthetic data generation and to empirically evaluate the performance of the eight Eigendecomposition parameters and the DPCA-ATI metric as moving target detection metrics. Briefly, the ESR was a conventional high resolution X-band SAR, except that the main antenna was split into two halves to provide monopulse capability. Two additional horn antennas were mounted on the aircraft about 1.10 metres in front and behind the centre of the main antenna. Together with the two halves of the main antenna the two horns provide a three beam interferometer.

The signals from each antenna were processed into complex valued SAR images. Exactly the same processing parameters and processor were used to generate each image ensuring that any phase errors introduced by the processor were the same for each image. These images are analytic images in complex form and there is a systematic phase shift between them due to physical separation between the receiving antennas both along the aircraft track and across track. Phase errors due to aircraft motion and across-track separation were removed using a technique described in [5].

An example of the three modulus images (corresponding to the fore, mid and aft antennas) used in this work is shown in Figure 1; the example is from the aft channel. The image is 250 pixels square, the range direction is upwards and the spatial resolutions on the sea surface are 1.04m in range and

$$\begin{aligned}
U &= B(\psi)C(\theta)D(\phi)P^2P^1 \\
&= \begin{pmatrix} c\psi & s\psi & 0 \\ -s\psi & c\psi & 0 \\ 0 & 0 & 1 \end{pmatrix} \begin{pmatrix} 1 & 0 & 0 \\ 0 & c\theta & s\theta \\ 0 & -s\theta & c\theta \end{pmatrix} \begin{pmatrix} c\phi & s\phi & 0 \\ -s\phi & c\phi & 0 \\ 0 & 0 & 1 \end{pmatrix} \begin{pmatrix} e^{i\delta_1} & 0 & 0 \\ 0 & e^{-i\delta_1} & 0 \\ 0 & 0 & 1 \end{pmatrix} \begin{pmatrix} e^{i\delta_2} & 0 & 0 \\ 0 & 1 & 0 \\ 0 & 0 & e^{-i\delta_2} \end{pmatrix} \quad (5)
\end{aligned}$$

0.84m along track. The three images used in this work show the radar return from a buoy in the southern North Sea together with a breaking swell wave identified in Figure 1 by the green and red ellipses respectively. The buoy is approximately 6m in height above the water surface. Back-scattering occurs at various points on the buoy. These points move with different speeds due to the rocking motion on a background swell and these points are mapped onto the image with different azimuth shifts which is why the buoy image is elongated along-track. The scatter cross-section at a number of points along the breaking wave is comparable with the buoy cross-section and any conventional detection algorithm based on a single image will have difficulty detecting the buoy (or any similar target) in such circumstances due to the multiplicity of false alarms.

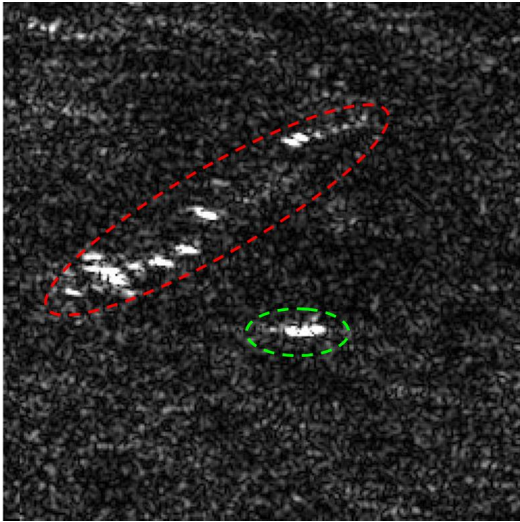


Fig. 1. ESR aft channel modulus image

B. Simulated Data Generation

In order to estimate the required detection threshold for a given Eigendecomposition parameter to achieve a specified false alarm rate we require a large number of three-channel clutter samples to approximate the marginal p.d.f. for the parameter. In this work these samples are generated as correlated samples from a stationary zero-mean complex Gaussian process.

In order to generate simulated sample covariance matrices, the parameters of the true covariance matrix of the underlying clutter process must be chosen. In this work the background was assumed to be stationary and homogeneous, i.e. $\phi_1 = \phi_2 = 0$. The simplifying assumption is also made that $\sigma_1 = \sigma_2 = \sigma_3$, i.e. the three channels are balanced in power. This is

quite reasonable from an engineering point of view as it simply requires that the channel gains be adjusted appropriately as was done in the case of the ESR data introduced above.

In order that synthetic data was generated which is both representative of realistic SAR data and allowed the calculation of thresholds which can be used to test the detection metrics against the ESR data, where possible, all required parameters were estimated from the three ESR images. The clutter power values were taken to be $\sigma_1 = \sigma_2 = \sigma_3 = 0.8$, the mean amplitude of the three coherent images, and the correlations ρ_1 and ρ_2 were calculated to be 0.75 and 0.56 respectively. In the real and simulated data each SAR image is formed from a single look, i.e. $n = 1$.

Given the parameters of the underlying covariance matrix for clutter only pixels, a large number of clutter only sample covariance matrices can be generated. For each sample covariance matrix the Eigendecomposition parameters and DPCA-ATI metric can then be calculated. The histogram of each of these parameters can then be used to approximate the p.d.f. of the parameter. A threshold can then be calculated such that the probability of the parameter exceeding the threshold for a clutter only sample covariance matrix is a specified value.

IV. APPLICATION OF EIGENDECOMPOSITION TO ESR DATA

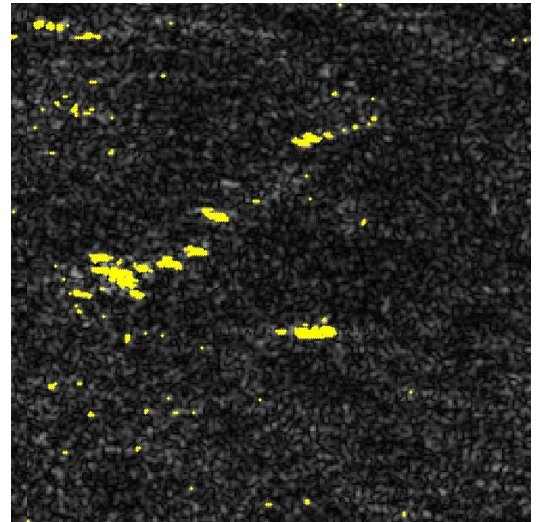


Fig. 2. ESR moving target detections using λ_1 , $P_f = 10^{-4}$

Using the theoretical clutter only sample covariance matrices, moving target detection thresholds were calculated for each Eigendecomposition parameter and the DPCA-ATI

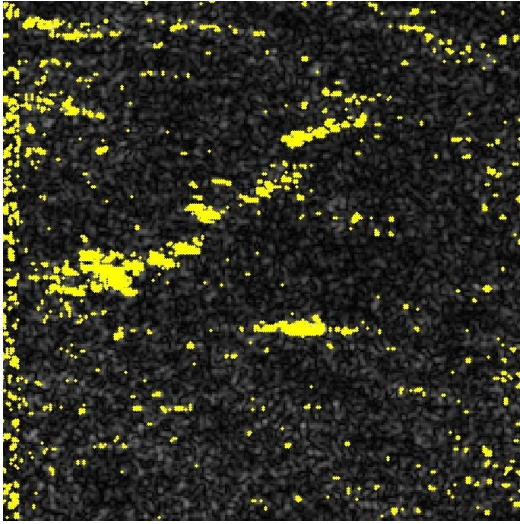


Fig. 3. ESR moving target detections using DPCA-ATI, $P_f = 10^{-4}$

metric for a false alarm rate of $P_F = 10^{-4}$. The Eigendecomposition parameters and DPCA-ATI metric of the sample covariance matrix for each set of three corresponding pixels in the ESR data were compared to this threshold. For each parameter, any pixels exceeding the threshold were declared as detections. For seven of the Eigendecomposition parameters almost no detections are declared and in cases where detections are declared they do not fall on pixels covering either the buoy or the breaking wave. However, the largest Eigenvalue λ_1 declares many pixels falling on both the buoy and breaking wave as detections and very few pixels elsewhere. This suggests that the majority of moving target information contained in the sample covariance matrix is concentrated into λ_1 by the Eigendecomposition and that this parameter is an effective moving target detection metric with a low false alarm rate. Figure 2 shows the pixels declared as detections by λ_1 .

When compared to the pixels declared as detections by the DPCA-ATI metric, shown in Figure 3, we see that λ_1 declares both less non-target pixels as detections and less buoy and breaking wave pixels as detections, i.e. λ_1 has both lower real-world probabilities of detection and false alarm than DPCA-ATI.

V. APPLICATION OF ICA TO ESR DATA

ICA [6] is a computational method for separating a multivariate signal into additive subcomponents. The method assumes that the sub-signals which are added together are mutually statistically independent and at most one of them has Gaussian first-order statistics. When these assumptions are met, ICA is a very effective solution to the problem of blind source separation. There are two main motivations for applying ICA to the three-channel ESR data presented above. Firstly, the SAR image formation process means that the complex value of any given pixel may be a sum of energy returned from multiple scatters in the scene and, hence, identifying targets of interest in the image requires the separation of energy returned

from both target and background scatters. Secondly, in a multi-channel system moving targets should be distinguishable from background scatters by their differing phase histories. This means that the first order statistics of the energy returned in the three-channels from a moving target should be different from that of background scatters. Furthermore, it is reasonable to hypothesise that these first order statistics will be independent as they are due to the physically independent motion processes of the target and clutter.

ICA is, in general, unable to identify the actual number of source signals. In this work we choose to analyse three components. This choice was motivated by the assumption that there are independent statistical processes generating the returns from the clutter background, the breaking wave and the buoy and that there are no other scatters in scene. ICA can be applied to the ESR data by considering each image to be a sample of a random vector which is assumed to be the sum of three independent components. More formally, each image is a vector of pixel values $\underline{x}_i = [|x_{i,1}|, |x_{i,2}|, \dots, |x_{i,62500}|]$ and is assumed to be generated as a sum of the real valued vector components $\underline{s}_1, \underline{s}_2, \underline{s}_3$:

$$\underline{x}_i = a_{i,1}\underline{s}_1 + a_{i,2}\underline{s}_2 + a_{i,3}\underline{s}_3 \quad (6)$$

weighted by real mixing weights $a_{i,k}$. In order to distinguish moving targets from background clutter we are interested in the pixel values in each of the three independent component images $\underline{s}_1, \underline{s}_2, \underline{s}_3$.

The FastICA algorithm [7] was used to separate the ESR data into independent components. This is a popular implementation of ICA due to its efficiency. The most significant feature of the algorithm is its use of maximisation of non-Gaussianity of signals as a measure of statistical independence.

Figure 4 shows the value of each pixel in the three independent components. Figure 5 shows the corresponding histograms of pixel values. The pixel values in the third independent component visually resemble background clutter and there are no strongly discernible patterns within the image. Furthermore, the distribution of pixel values across the image closely fits a Gaussian curve which is consistent with the independent component representing background clutter. In the first independent component the values of pixels covering the buoy are strong outliers within the image and there are no other strong outlier pixels. Of most interest is the second independent component which shows that not only are the pixel values corresponding covering both the buoy and the breaking wave outliers to the distribution of pixel values across the image, but they are outliers at opposite ends of the spectrum and are hence distinguishable in the image. One possible explanation for this is that the second component is sensitive to across track velocity. The breaking wave and buoy have different across track velocity values whilst the background clutter is stationary and would hence have different pixel values in an independent component sensitive to this physical phenomenon.

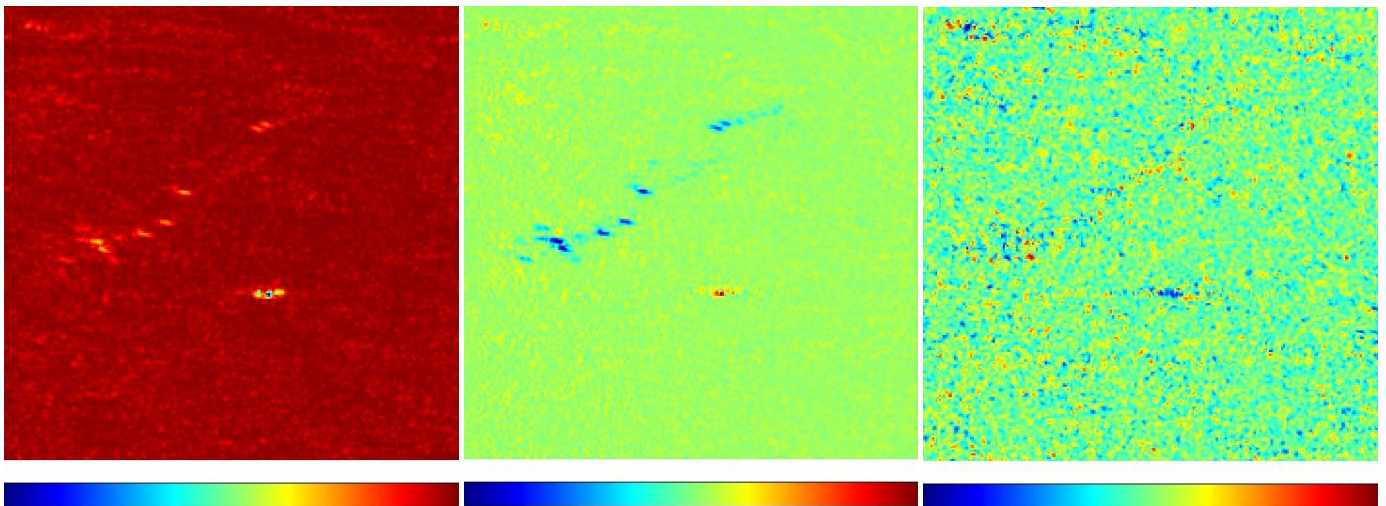


Fig. 4. ICA component pixel values

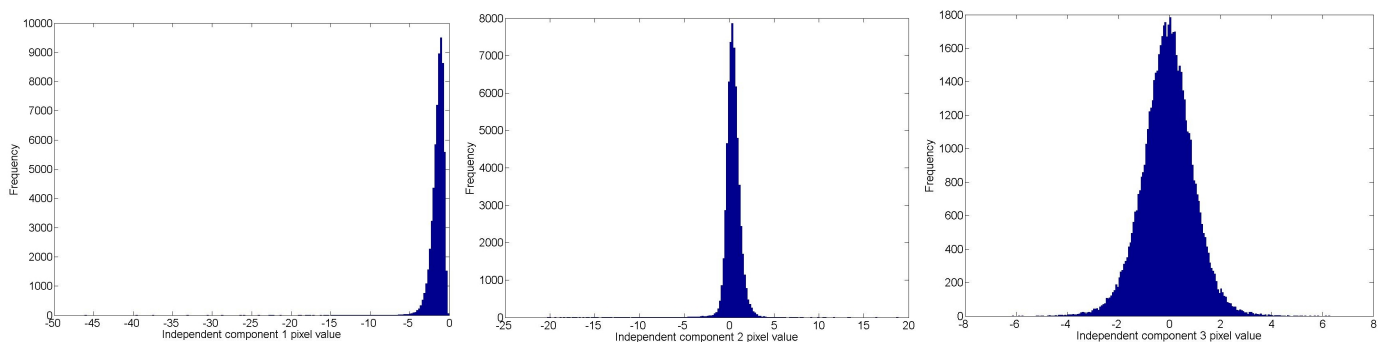


Fig. 5. ICA component pixel value histograms

VI. CONCLUSION

In this paper a new deterministic method for finding the parameters of an Eigendecomposition of a 3×3 Hermitian matrix has been presented. Based on a theoretical model of clutter, simulated clutter samples were generated and used to estimate a constant false alarm rate (CFAR) threshold for each Eigendecomposition parameter as a moving target detection metric. These thresholds allowed the evaluation of the eight Eigendecomposition parameters as GMTI metrics using real maritime SAR data. Experimental results suggest that the majority of the moving target energy is contained within the largest Eigenvalue. Furthermore, it has been shown that the largest Eigenvalue can achieve a high real-world probability of moving target detection with a low probability of false alarm. ICA has been shown to be an effective method for separating the intensity energy in three-channel SAR imagery due to moving targets from the energy due to background clutter and that the mixing weights of the independent components can allow the separation of different classes of moving target.

VII. ACKNOWLEDGEMENT

This work was supported by the MOD University Defence Research Centre on Signal Processing.

© British Crown Copyright - Dstl 2010 - published with the permission of the Controller of Her Majesty's Stationery Office

REFERENCES

- [1] C. Gierull, "Statistics of SAR interferograms with application to moving target detection," Defence Research and Development, Canada, Tech. Rep. TR 2001-045, Jul. 2001.
- [2] S. Chiu, "A simulation study of multi-channel RADARSAT-2 GMTI," Defence Research and Development, Canada, Tech. Rep. TR 2006-209, Nov. 2006.
- [3] I. Sikaneta and J.-Y. Chouinard, "Eigendecomposition of the multi-channel covariance matrix with applications to SAR-GMTI," *Signal Processing*, vol. 84, no. 9, pp. 1501–1535, 2004.
- [4] E. Anastassakis, "A geometrical method for diagonalizing real, symmetric 3×3 matrices through Euler rotations," *Applied Mathematics and Computation*, vol. 117, no. 2-3, pp. 193–201, 2001.
- [5] B. Barber, "Multichannel ATI-SAR with application to the adaptive Doppler filtering of ocean swell waves," *IEE Proc-Radar Sonar Navig.*, vol. 150, pp. 403–410, 2003.
- [6] P. Comon, "Independent Component Analysis: a new concept?" *Signal Processing*, vol. 36, no. 3, pp. 287–314, 1994.
- [7] A. Hyvärinen, "Fast and robust fixed-point algorithms for independent component analysis," *IEEE Trans. Neural Netw.*, vol. 10, no. 3, pp. 626–634, 1999.